# EFFECTS OF OPTICAL CROSSTALK IN CCD IMAGE SENSORS

R. H. Dyck
Fairchild MOS/CCD
4001 Miranda Ave.
Palo Alto, CA.

W. Steffe
Fairchild MOS/CCD
4001 Miranda Ave.
Palo Alto, CA.

## ABSTRACT/INTRODUCTION

It is a well-known phenomenon in silicon image sensors that a significant level of optical crosstalk occurs at wavelengths longer than approximately 750nm and that this crosstalk is due to the lateral diffusion of minority carriers generated below the depleted portion of the silicon substrate. In addition, a low level of optical crosstalk can occur at all wavelengths due to scattering and light-piping in the thin film portion of the device. This paper describes these effects quantitatively as they occur in several different types of image sensors produced at Fairchild. Comparisons with predicted values are also made. Finally, the impact of these effects on device performance in practical applications is discussed.

## THE MODEL FOR INTERNAL SPECTRAL RESPONSE

Before describing the crosstalk model used for the various predictions, it is instructive to look at the basic model for internal spectral response, i.e., for the response of the silicon device assuming 100% transmittance at the surface. This is a one dimensional model consisting simply of a depletion layer at the surface and, below this, a semi-infinite neutral region of uniform minority carrier diffusion length. Figure 1 shows the general equation and a resulting spectral response for particular values of the depletion depth ($L_D$) and the diffusion length ($L_N$, for an n-channel device). Also shown in the figure is the portion of the response due to diffusion. It is this portion of the response that gives rise to virtually all of the crosstalk observed in silicon imaging devices. The diffusion response is predominant in the infrared because the absorption length ($\alpha^{-1}$) is the greatest at these wavelengths. Depletion depths of 7 to 10μm are typical in Fairchild charge-coupled imaging devices. In general in CCD's, this depletion depth is modulated by the gate potential as it is clocked; a time average is then assumed. Diffusion lengths of 50 to 100μm are also typical, judging from the response values typically observed. (Because of back-contact recombination and a typical substrate thickness of 200μm, longer diffusion lengths do not change the response much.

## MODEL FOR DIFFUSION CROSSTALK

Consider an infinitesimal diameter beam of collimated monochromatic radiation at normal incidence on a large area imaging device. Photoelectrons generated in the neutral region will, on the average, diffuse laterally a distance comparable with the depth of generation measured from the top of the neutral region and then be collected in the depletion region at the nearest potential minimum. Figure 2 depicts this process; it is the basis of the crosstalk model. The model neglects any reduction of the depletion depth or absence of depletion at the channel-stop boundaries between elements. The assumption of normal incidence can be made because even with small f/no. optics the high refractive index in silicon (>3.5) results in substantial internal collimation normal to the surface.

The most generally useful form of the characterization of this crosstalk is the modulation transfer function (MTF) factor (output modulation/input modulation). This is obtained by integrating the above spreading process over a sine-wave modulated large area of irradiation. The mathematical treatment of this problem has been given by Seib, (Ref. 1).

An example result is shown in Figure 3 for the case of $L_D$ = 10μm and $L_N$ = 100μm. From this example one can see the most prominent

feature of the optical crosstalk characteristic of most silicon imaging devices, namely a large decrease in MTF as the wavelength is increased from approximately 800nm to approximately 900nm. This large decrease occurs at spatial frequencies as low as approximately 10 line pairs/mm. (Because the absorption coefficient increases slightly with temperature, these curves should be corrected for large departures from room temperature; see Table.)

The MTF is also affected by the optical aperture of the elements. Thus, if the integrated response of the array is uniform over the entire area; i.e., if there is no loss of response between the elements, and if the boundary region is negligibly small, the MTF is given by

$$\frac{\sin X}{X} \quad \text{where } X = \frac{\pi f}{2 f_N}$$

and where $f_N$ is the Nyquist frequency---the maximum resolvable frequency. In this idealized case the MTF is 0.637 at $f_N$. If the boundary region is finite, there will be a further reduction in the MTF. An example of a resultant family of MTF curves for one device is shown in Figure 4; this is for a line-scan device with a 13μm element spacing and with 5μm neutral channel stop regions between the primary depleted portions of the elements, (Ref. 2). In these channel stop regions the carriers are virtually all collected at one or the other of the two adjacent depletion regions and the partitioning of the response is proportional to the distance from the far side of the channel stop. (The data in the figure is discussed later in this paper.)

## MAJOR EFFECT OF DIFFUSION CROSSTALK IN DIFFERENT IMAGE SENSORS

In area image sensors of the frame-transfer type and the time-delay and integration (TDI) type, the only effect of diffusion crosstalk is on MTF. In line-scan image sensors a second effect is significant, namely, infrared response in the opaqued CCD readout register(s). In normal operation this produces a uniform black-level offset in the output signal that is modulated by the integrated image intensity. Thus, the black level will be relatively accurate when only a small fraction of the elements are exposed to a high illumination level, but may have a significant error when most of the elements are exposed to the high illumination level. Associated with this register response is a loss of infrared response at the photoelements. A typical predicted photoelement response, with the corresponding predicted total response for the one-dimensional model, is shown in Figure 5. The maximum shift register crosstalk occurs when most of the array is irradiated at the highlight level.

In interline-transfer (ILT) area imagers (Ref. 3), there are opaqued vertical registers interdigitated with columns of sensor elements; crosstalk into these registers leads to an analogous effect, namely, vertical image smearing. For example, crosstalk from an intense spot image will, because of the way the device is clocked, result in a uniform increase in signal in all the charge-packets moving through the adjacent shift registers. At the display this increase in signal will appear as a vertical smear which is uniform over the full height of the picture. Figure 6 shows a schematic cross-section of the device. Whereas in the line-scan device described above, the metal extends from the opaqued registers over the photoelements by 11μm, in ILT area imagers it is necessary to employ much smaller dimensions of 2μm to 6μm. The reason for holding this dimension small is that it directly affects the responsivity of the device and/or the cell size. In the Fairchild CCD211, a 244 X 190 element ILT image sensor with a horizontal cell dimension of 30μm and a horizontal aperture of 14μm, an increase of overlap from 2μm to 6μm would result in a decrease in responsivity of more than 50 percent. Figure 7 shows how the level of the smear signal in the CCD211 varies with wavelength. Here a parameter called the charging ratio (r), is plotted; the inset in the figure shows how the smear signal varies with this ratio and the size of the bright spot causing the smear. The charging ratio is the ratio of the shift register photocurrent, caused by crosstalk, to the photoelement current.

The predicted curve in Figure 7 shows that at 600nm the charging ratio should be less than one percent. However, as shown in the figure, typical devices have a charging ratio of approximately two percent. This excess is also seen to be more or less independent of wavelength. This excess crosstalk is attributed to optical scattering in the polysilicon gate; the scattering could occur both at oxidized grain boundaries and at sloped edges of any of the exposed polysilicon layers.

## METHODS OF MEASUREMENT

Crosstalk measurements with a light spot image and with bar-pattern images have been made with a B&L metallurgical trinocular microscope head mounted on rails over a large mechanical stage. The device and socket are mounted rigidly to the stage. The third eyepiece tube holds either the light spot source or a small projector box equipped with lamp, diffusers, filter holders and the mask holder.

The spot source is a Sylvania C2T lamp with a circular incandescent source of approximately 100μm diameter. Small-aperture baffles at several points along the optical path minimize flare. Intensity is controlled with a pair of crossed polarizers. Both B&L and Nikon 20X objectives have been used successfully to obtain crosstalk values on 13μm-pitch-arrays of approximately 3% for the nearest neighbor element. This low level of crosstalk (at short wavelengths) establishes the quality of the optical system.

Only narrow-band and medium-band measurements are considered definitive with this system, no attempt has been made to achieve a spectrally flat system as would be required with calibrated broadband sources. For each filter the system is refocused when using refractive objectives.

For characterization of device crosstalk vs. wavelength, it is desirable to have optics that are not affected by wavelength; that is, to have a reflective objective. A Beck-Ealing 15X reflective objective was used for such measurements. For best results care should be taken that the reflective elements have been properly aligned. In the measurements described here, using a light spot that would ideally have had a diameter of approximately 5μm, and making a short wavelength ($\leq$600nm) measurement on a 13μm-pitch array, the nearest-neighbor signal read 7% instead of the 3% obtained with the best refractive objective, and the second nearest neighbor read 2% instead of <0.5%.

In all of the data presented here, those taken with the reflective objective were corrected while those taken with the refractive objectives are assumed not to need correction.

All data were taken on photoelements near the preamplifier of the device so that charge transfer inefficiency was negligible.

## MTF CHARACTERIZATION OF THE CCD121H AND CCD131

In order to make MTF measurements, one should ideally have a sine-wave modulated image of known amplitude. However, such a source was not available for the measurements described here. Instead, it was decided to use a chrome mask (which would ideally produce a square-wave modulated image) and then determine at what spatial frequency the 15X reflective objective would blur this into approximately sine-wave modulation. Since light spot measurements showed that the image sensor was operating within a few percent of ideal performance at short wavelenghts ($\leq$600nm), the problem became one of finding the spatial frequency where the measured data matched the predicted performance. This was found to occur at 0.67 $f_N$ (25 lp/mm) within experimental accuracy. Next the output modulations were measured at the longer wavelengths at this one spatial frequency. The ranges of the data for several typical devices are shown in Figure 4. The agreement with theory is not as good as the estimated precision of measurement which is $\pm$ 10%; in the 700-800nm range, the experimental values of MTF are lower than predicted; at 1000nm they are higher.

In a previously published paper, Vicars-Harris (Ref. 4), presents square-wave response (CTF) data for a sample device of this same type, i.e., a Fairchild line-scan CCD image sensor with 13μm elements. It is of interest to compare the two sets of data. The Vicars-Harris data includes the losses due to the lens and, even though the lens is recognized for its high resolution---it is a 3 inch B&L Super Baltar---the relative response is significantly lower. For example, in a 700-800nm band, the Vicars-Harris CTF value at 25 lp/mm (0.67 $f_N$) is 53%, while our corresponding MTF value (the average of 700nm and 800nm values) is 63%.

## LIGHT SPOT CHARACTERIZATION OF THE CCD121H AND CCD131

While it is possible in principle to use MTF data to compute the spread function for a light spot, it is of interest to measure some directly. Figure 8 shows light spot data for light spot diameters significantly less than the element size; the spot diameters are only approximate. From this data it may be seen, for example, that at 900nm the second-nearest neighbors receive a signal which is 7.5% of that of the center element.

## PREDICTED PERFORMANCE FOR AN ADVANCED ILT IMAGE SENSOR

As described above (see Figure 7), the ILT type of image sensor exhibits vertical smearing due to crosstalk into the vertical registers. Given that the CCD211 in Figure 7 has a charging ratio of 15% at 800nm, it is desirable to improve the design so as to reduce this value to the order of one percent or less. Increasing the metal overlap over the photoelements should help somewhat, but the largest gain should come by increasing the depletion depth. Unfortunately, current material and processing constraints on substrate doping for good manufacturability limit the minimim doping level to approximately 1 X $10^{14}$/$cm^3$ (130Ω-cm). Similarly the voltage that can be applied across the depletion layer is limited by considerations of manufacturability; a realistic goal is 20V. The result is an increase in depletion depth from 7μm to 17μm. In a new design, which also includes an antiblooming sink stripe adjacent to each column of photoelements, the predicted charging ratio at 800nm is reduced approximately three fold---not as much as desired, but nevertheless a significant decrease. The improvement is shown in Figure 9 where, instead of showing monochromatic data, we show broadband data as a function of long-wavelength cutoff, achieved with an external filter. Characterized this way at a cutoff wavelength of 800nm, the charging ratio is decreased in the new design from 4% to approximately 1%. Thus, a bright spot with a diameter of 1% of picture height would cause a smear signal of 1 X $10^{-4}$ times the spot signal.

## SUMMARY

Diffusion crosstalk can severely limit the performance of CCD image sensors at wavelengths beyond approximately 850nm. This performance limitation has been discussed in detail for several imaging devices. Both the crosstalk to neighboring photoelements and that to adjacent shift registers can be significant.

## REFERENCES

1. D. H. Seib, "Carrier Diffusion Degradation of Modulation Transfer Function in Charge Coupled Imagers", IEEE Trans. El, Devices ED-21, March, 1974, pp. 210-17.

2. The CCD121H and CCD131 are two-register line-scan devices with 1728 elements and 1024 elements, respectively.

3. For a detailed description of an ILT device, see the paper by W. Steffe, L. Walsh, and C. K. Kim, "A High Performance 190 X 244 CCD Area Image Sensor Array", Proc. of the 1975 International Conference on the Application of CCD's, NELC, San Diego, October 29-31, 1975, pp. 101-108.

4. M. Vicars-Harris, "Slow Scan Operation of Long Linear CCD Arrays", Proc. of the Symposium on CCD Technology for Scientific Imaging Applications, JPL, Pasadena, March 6-7, 1975, pp. 175-85.

## ACKNOWLEDGEMENTS

The computer programs for the MTF and the infrared smearing were developed by Harold Hosack. Refinements and additions to these programs were made by Peter C. Chen.

TABLE: ABSORPTION LENGTH OF SILICON AT TWO TEMPERATURES

| $\alpha^{-1}$ (um) | λ (nm) | |
|---|---|---|
| | 300°K | 77°K |
| 2.5 | 600 | 540 |
| 5 | 705 | 605 |
| 10 | 795 | 715 |
| 25 | 880 | 815 |
| 50 | 940 | 870 |
| 200 | 1000 | 940 |
| 1000 | 1060 | 980 |

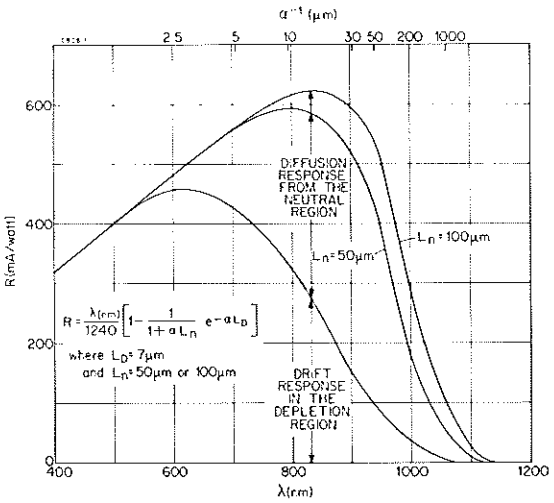


Fig. 1 Theoretical internal spectral response based on a one-dimensional model

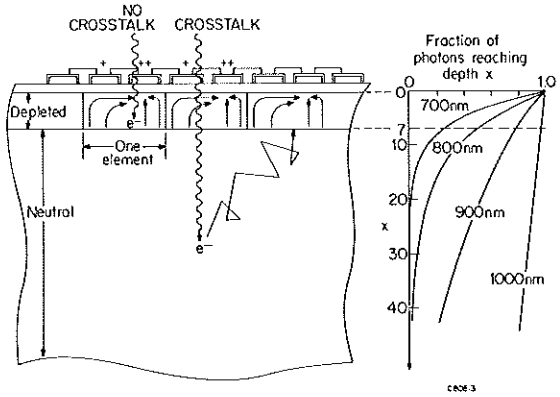


Fig. 2 The optical crosstalk process

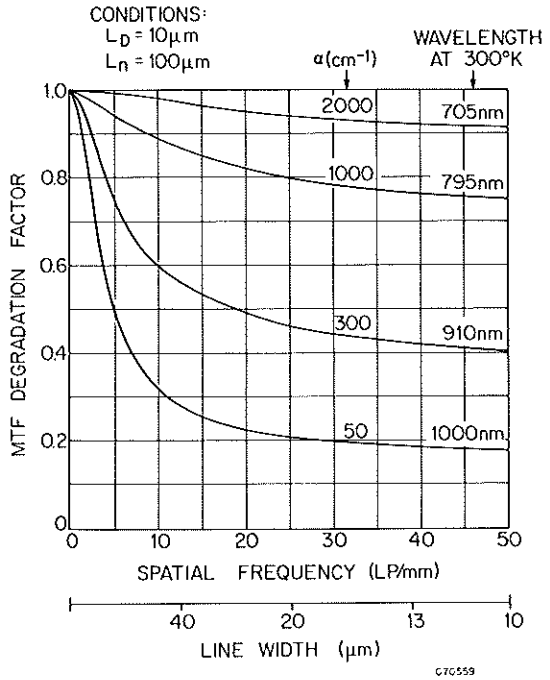


Fig. 3 Calculated MTF degradation factor vs. spatial frequency and wavelength

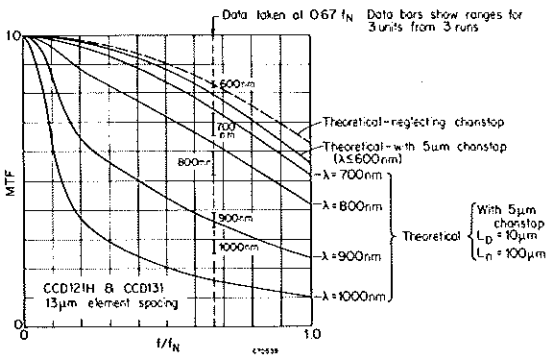


Fig. 4 In-phase MTF vs $f/f_N$ for a line-scan image sensor

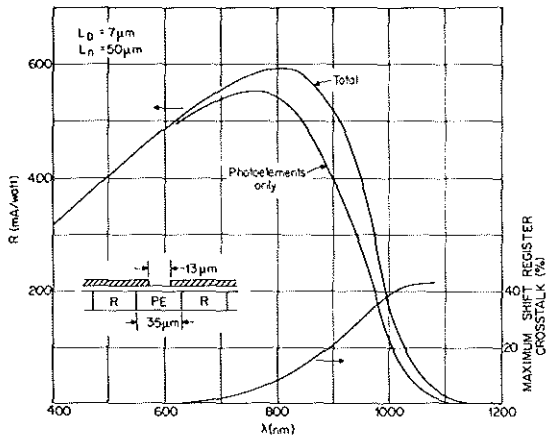


Fig. 5 Theoretical internal spectral response for the CCD131 line-scan image sensor

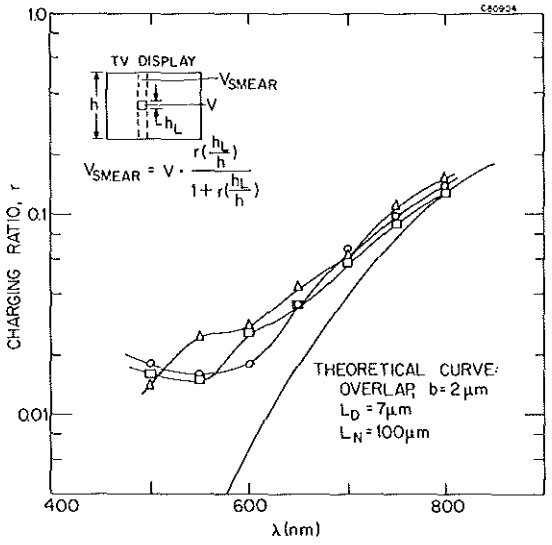


Fig. 7 Charging ratio vs. wavelength for three typical CCD211 ILT image sensors

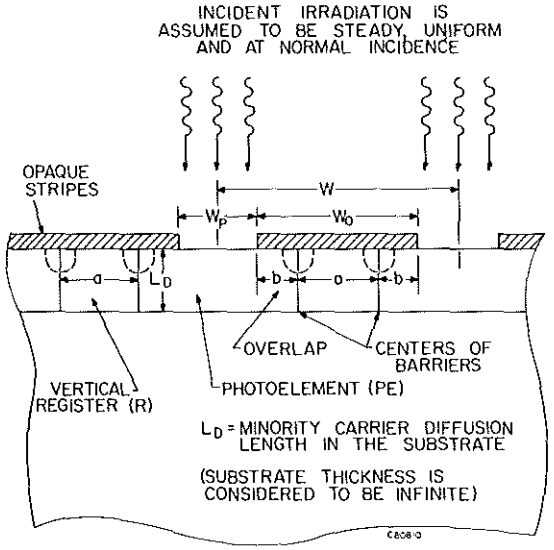


Fig. 6 Model for the calculation of deep carrier crosstalk in an ILT image sensor

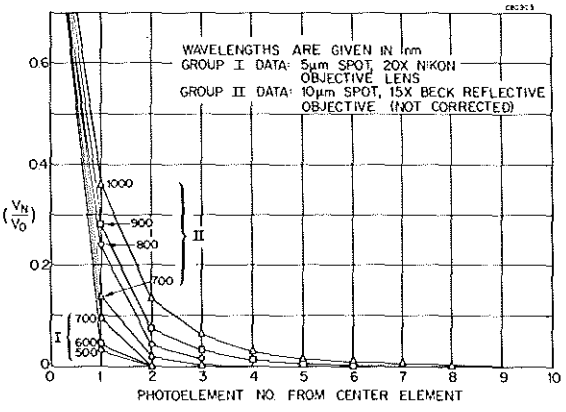


Fig. 8 Optical crosstalk of a typical CCD121H line-scan image sensor characterized using a light spot

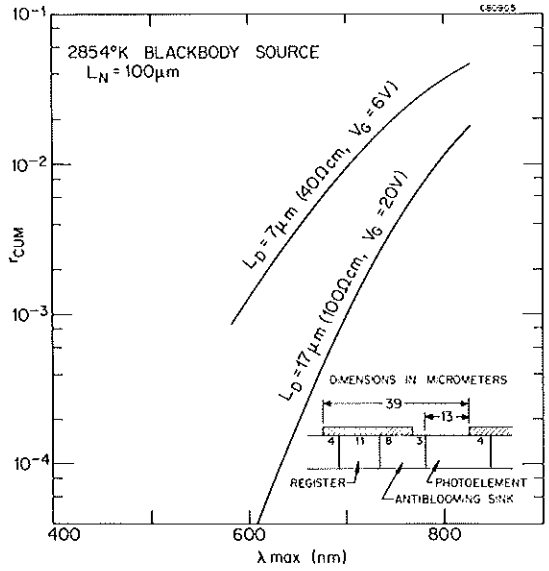


Fig. 9 Cumulative charging ratio vs. cut-off wavelength